Heliyon 5 (2019) e01742

Contents lists available at ScienceDirect

Heliyon

journal homepage: www.heliyon.com

Hydrocarbon reservoir characterization and discrimination using well-logs over "AIB-EX" Oil Field, Niger Delta

Ibukun Olorunniwo, Sunday J. Olotu *, Olatunbosun A. Alao, Adekunle A. Adepelumi

Obafemi Awolowo University, Ile-Ife, Nigeria

ARTICLE INFO

Keywords:
Earth sciences
Reservoir characterization
Discriminant tool
Crossplot
Bi-variate
Tri-variate

ABSTRACT

A computerized advanced statistical analysis which involves the characterization of reservoir elements involving mapping of lithofacies and pore fluids through crossplots of basic seismic variables in both bi-variate and tri-variate domains and functional transformations including rotation of axes have been used as discriminant tools over "AIB-EX" Oil Field, Niger Delta.

The methodology encompasses reconstruction of geologic lithofacies information from geophysical logs. Reservoir characterization, rock physics analysis and log inversion were carried out using IHS Kingdom Advanced and Origin software. Three reservoir zones namely A, B, and C were analyzed.

The obtained results characterized the reservoir elements as: shale, sandy-shale, shaly-sand and sand (with respective GR counts and P-wave velocity of 105–125 API and 2400–3600 m/s, 75–105 API and 2100–5000 m/s, 45–75 API and 2200–4750 m/s, and 10–45 API and 2000–4600 m/s) which represents seismic scale sedimentary units called lithofacies. Also, the results of both the bi-variate crossplots (GR and P-wave velocity) and tri-variate crossplots (GR, P-wave velocity, and resistivity) have not only differentiated the different lithology but have discriminated the saturating fluid (water or hydrocarbon). The pore fluids were further characterized as either brine or oil based on powerful discriminant tools such as plots of acoustic impedance versus porosity and elastic impedance versus porosity.

Conclusively, the result of the research confirmed that hydrocarbon reservoirs can be discriminated with varying degree of effectiveness in various domains using the adopted approach. The obtained result, which can also be used to calibrate seismic inversion, yielded a reliable seismic lithofacies map in the presence of high resolution 3-D seismic data.

1. Introduction

Previously, reservoir characterization was mostly deterministic, basically quick look method of log interpretation as well as petrophysical analysis. Today, proper reservoir discrimination and characterization of its lithology along with its fluid-content requires quantitative techniques of log studies and seismic inversion methods. These factors led to discriminating and characterizing the delineated reservoirs in the study area. However, this research investigated the discrimination of hydrocarbon reservoirs from borehole log studies to obtain seismic lithofacies templates that would be useful as mapping tools for reservoir characterization and discrimination.

Therefore, interpretation of reservoir parameters has moved from being primarily qualitative to largely quantitative. Previous works have shown different tools such as, the ratio of P-wave velocity to S-wave velocity, impedances and lambda-mu-rho variable in characterizing and discriminating reservoirs (Hilterman et al., 1998; Castagna et al., 1998). The crossplots of the ratio of P-wave velocity to S-wave velocity and Poisson's ratio versus acoustic impedance have been used for lithology discrimination in the Gulf of Mexico. The impedances (P-impedance, S-impedance, Poisson impedance and elastic impedance) crossplotted with other reservoir parameters have been studied for identification of lithology, discrimination of fluid content within the reservoir and characterization of the quality of pay zone (Hilterman et al., 1998; Mazumdar, 2007; Conolly, 2007). Rotimi et al. (2014) modeled lateral heterogeneity in reservoirs using the multivariate analysis and Blouin et al. (2017) estimated porosity in Fort Worth Basin using Bayesian simulation framework with improved accuracy and efficiency. Also, Azevedo et al. (2014) and Azevedo et al. (2015) used the multidimensional scaling for evaluating of reservoir properties meanwhile Lai et al.

* Corresponding author.
E-mail address: jephotto@gmail.com (S.J. Olotu).

https://doi.org/10.1016/j.heliyon.2019.e01742
Received 15 September 2018; Received in revised form 8 February 2019; Accepted 13 May 2019

(2016) designed a model that uses GR, bulk density, neutron, and sonic logs and their ratios as variables to identify diagenetic facies from well logs. Additionally, Teh (2012) demonstrated reservoir characterization and simulation using geostatistical method while Maryam (2017) showed the importance of multivariate reservoir characterization modeling and facie analysis.

These discriminant parameters have been effectively used as powerful mapping tools for reservoir characterization and discrimination in this research work. The significance of these discriminant tools is that it had successfully mapped the lithofacies in the hydrocarbon reservoirs with varying degree of effectiveness in various domains along with its fluid contents. The main objective of this study is to present seismic reservoir

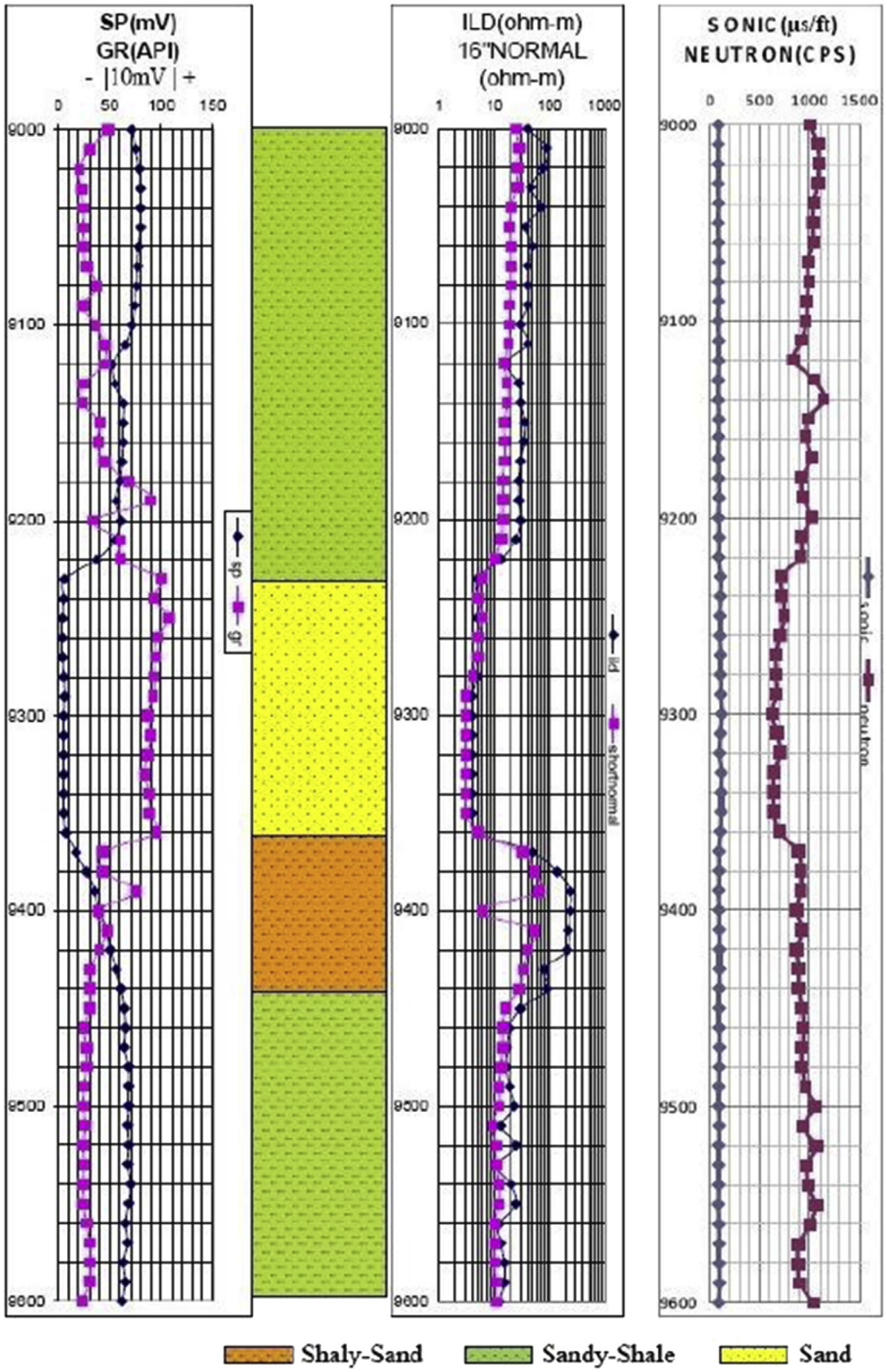

Fig. 1. Sample of logs from OBD-1 well showing different lithologies.

characterization and discrimination over "AIB-EX" Oil field, Niger Delta. Moreover, proper reservoir evaluation and management requires reservoir discrimination and characterization for proper lithology and fluid-content distribution.

2. Geological setting

The Niger Delta is a large, arcuate delta of the destructive, wave dominated type, situated on the continental margin of the Gulf of Guinea between latitudes 30° and 60° N and longitudes 50° and 80° E. The basin is a depositional frame within the southern Nigerian basin (Murat, 1972; Weber and Daukoru, 1975; Reijers, 1976). The Tertiary Niger Delta covers an area of about 75,000 sq. km and is composed of an overall regressive clastic sequence which reaches a maximum thickness of 30,000 ft [9,000 m] to 40,000 ft [12,000 m] (Evamy et al. 1978). Starting as separate depocentres, the Niger Delta has coalesced to form a single united system since Miocene (Short and Stauble, 1967). Evidence from all the deep wells in the Niger Delta shows that there is a lithostratigraphic succession in which a regressive sequence is properly defined. Short and Stauble (1967) have therefore divided the tertiary deltaic complex into three major facies units based on the dominant environmental influences.

These three main sedimentary environments or subsurface stratigraphic units are the continental, transitional, and marine environment. The Tertiary sequence in the Niger Delta consists of the three formations that are locally designated in ascending order (from the bottom) the Akata Formation, Agbada Formation, and Benin Formation. Amongst these three formations, the Agbada Formation constitutes the main reservoir for hydrocarbons in the Niger Delta (Short and Stauble, 1967; Frankl and Cordry, 1967).

3. Methodology

The data set for this study was obtained from "AIB-EX" Oil Field, Onshore Niger Delta. It consists six wells OBD-1, OBD-3, OBD-14, OBD-16, OBD-20 and OBD-22. The data for each well consists of a suite of logs namely; spontaneous potential (SP), gamma-ray (GR), resistivity [such as microspherically focused log (MSFL), shallow laterolog (LLS), deep laterolog (LLD), short-normal (16″ Normal) and deep induction (ILD) log], sonic and neutron logs. The suite of logs in each well were reconstructed to aid the subdivision of different lithologies (sand, shaly-sand, sandy-shale and shale) which were carried out based on qualitative log interpretation. Fig. 1 show a sample of the reconstructed logs for OBD-1 well and its different lithologies. The shale baseline was established first so that the lithologies could be precisely demarcated and identified in the section of interest. Then, the shale baseline was used as the reference in making measurements to determine the characteristics of sands and their formation waters.

Geophysical logs were analyzed using IHS Kingdom Advanced software and reservoirs were delineated by correlating log curve signatures from six wells in the study area.

Petrophysical parameters of the reservoirs were also obtained at each sample point across the depth of the six wells. Porosity, fluid saturation, and volume of shale content were determined from available well logs in the study area. However, the flushed zone resistivity (R_{xo}), true resistivity (R_t), porosity (ϕ) and water saturation (S_w) were obtained from resistivity logs while the volume of shale (V_{SH}) was obtained from gamma ray index (I_{GR}). The mud filtrate resistivity (R_{mf}) value was obtained from available log data.

Rock physics parameters such as P-wave velocity, S-wave velocity and density were modeled through multivariate regression analysis, which has been previously published (Olorunniwo et al., 2016). Extensive crossplot of the reservoirs parameters was then carried out using the Origin software.

4. Results and discussion

The log correlation of three reservoirs (A, B and C) across six wells is depicted in Fig. 2. The top of reservoir A is at depth of 4,110–4,350 ft (1,370–1,450 m) while its bottom varied at depth 5,370–5,550 ft (1,790–1,850 m); for reservoir B, the top occurs at depth of 6,800–6,840 ft (2,267–2,280 m) and its bottom is at depth of 9,270–9,450 ft (3,070–3,150 m); whereas for reservoir C, the top varied at depth 9,670–9,790 ft (3,223–3,263 m) and its bottom occurs at depth 10,100–10,650 ft (3,367–3,550 m). Therefore, it was observed that there is variation in the lateral extent across the wells of each reservoir. Reservoir A is thick and laterally extended, B is relatively thick, and C is thin. However, there is need to infer the termination of sands B and C in OBD-14 and OBD-16 wells because the available data is limited in those wells.

A plot of gamma ray (GR) against P-wave velocity for reservoirs A, B and C in OBD-1 well was used as a lithologic discrimination tool. It is pertinent to note that, though there is some varying degree of overlapping to separate clusters of the lithofacies but the bi-variate crossplots (Figs. 3, 4, and 5) identified and differentiated the lithofacies namely: black represented by sand, red for shaly-sand, green for sandy-shale and

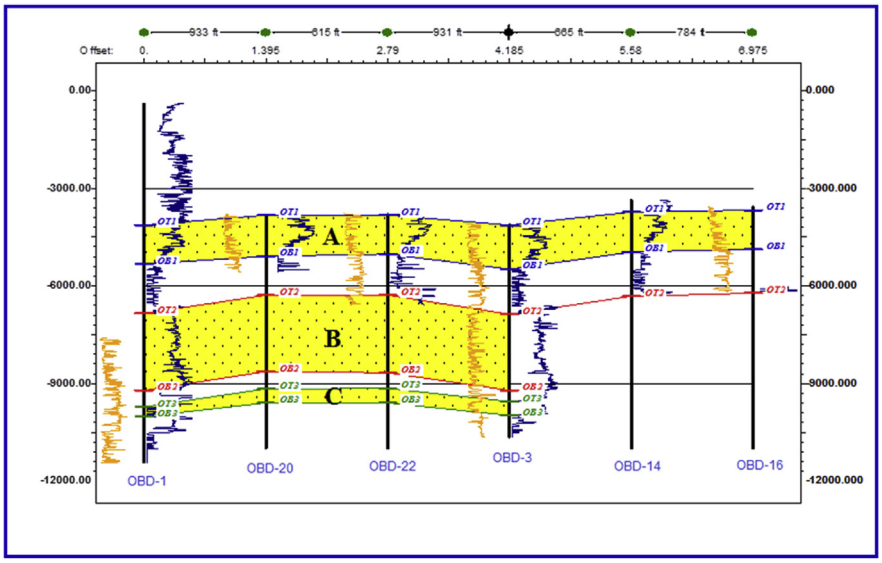

Fig. 2. Log correlation of reservoirs A, B and C across six wells [derived from IHS Kingdom Advanced].

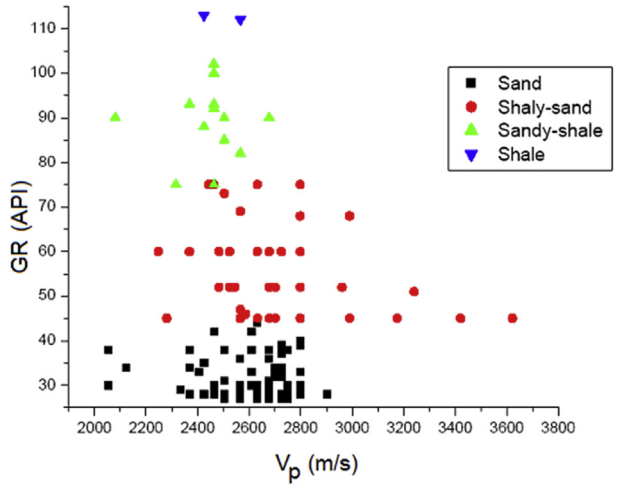

Fig. 3. The plot of GR versus P-wave velocity for reservoir A in OBD-1 well [derived from Origin 7.0].

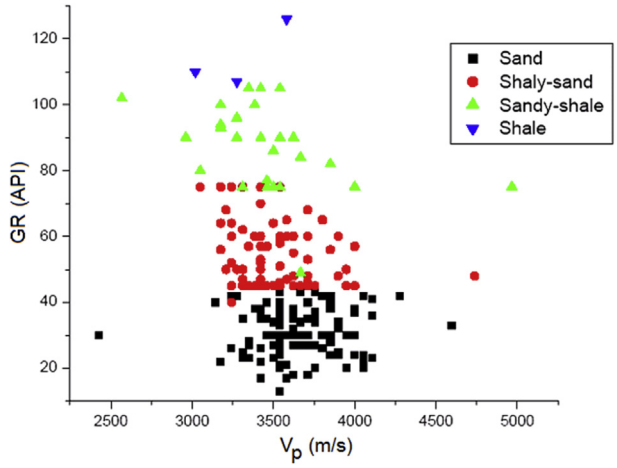

Fig. 4. The plot of GR versus P-wave velocity for reservoir B in OBD-1 well [derived from Origin 7.0].

blue represents shale by colour coding based on partitioning using gamma ray index (I_{GR}) serialization. Obviously, the sand falls within low GR counts (10–45 API) and low to moderate values of P-wave velocity (2,000–4,600 m/s); the shaly-sand has intermediate values of GR counts (45–75 API) and low to moderate values of P-wave velocity (2,200–4,750 m/s); the sandy-shale has moderate to high GR counts (75–105 API) and low to moderate values of P-wave velocity (2,100–5,000 m/s); and the shale exhibits high GR counts (105–125 API) and intermediate values of P-wave velocity (2,400–3,600 m/s). These lithofacies, however, fall within the same velocity regime.

Each lithofacies of these reservoirs were crossplotted together and compared. Figs. 6, 7, 8, and 9 show the plots of GR versus P-wave velocity (bi-variate crossplots) in comparing sand, shaly-sand, sandy-shale and shale of reservoirs A, B and C respectively in OBD-1 well, which compared the same lithofacies found in the reservoirs. For example, the plots show the exact range of values of GR counts and P-wave velocity peculiar to each lithofacies.

The tri-variate crossplots of GR, P-wave velocity, and resistivity comparing reservoirs A, B and C in terms of lithology and fluid saturation are shown in Figs. 10, 11, and 12. These figures also discriminate the different lithology as well as the saturating fluid (water or hydrocarbon) based on resistivity values, in which low values indicate water-saturated zones and high values confirm the presence of hydrocarbon in the reservoirs.

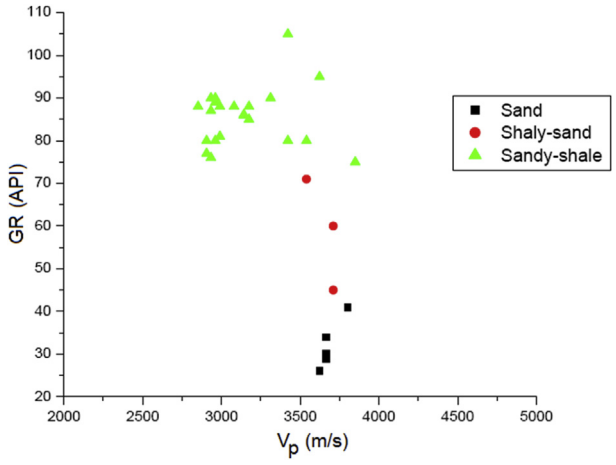

Fig. 5. The plot of GR versus P-wave velocity for reservoir C in OBD-1 well [derived from Origin 7.0].

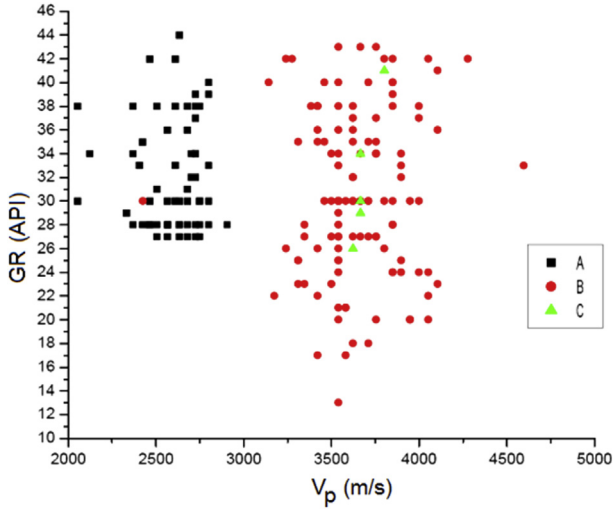

Fig. 6. The plot of GR versus P-wave velocity in comparing sands of reservoirs A, B and C in OBD-1 well [derived from Origin 7.0].

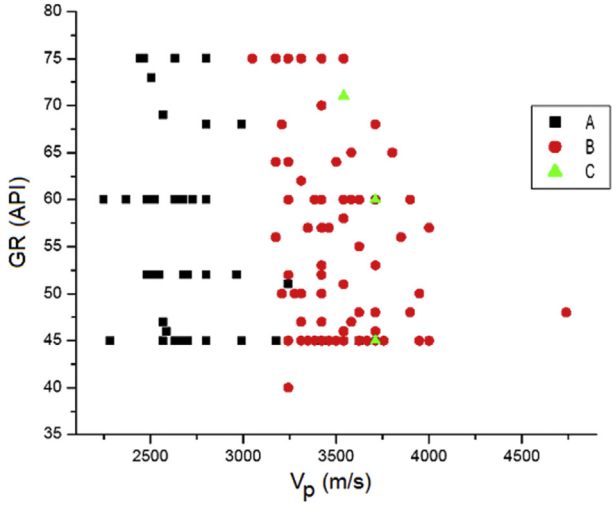

Fig. 7. The plot of GR versus P-wave velocity in comparing shaly-sands of reservoirs A, B and C in OBD-1 well [derived from Origin 7.0].

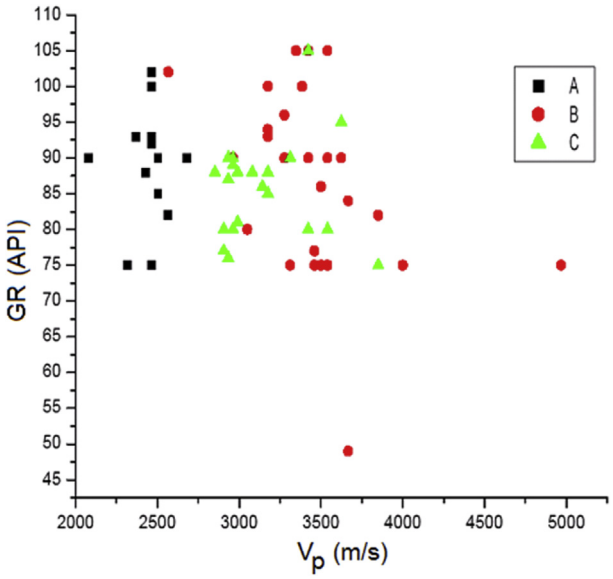

Fig. 8. The plot of GR versus P-wave velocity in comparing sandy-shales of reservoirs A, B and C in OBD-1 well [derived from Origin 7.0].

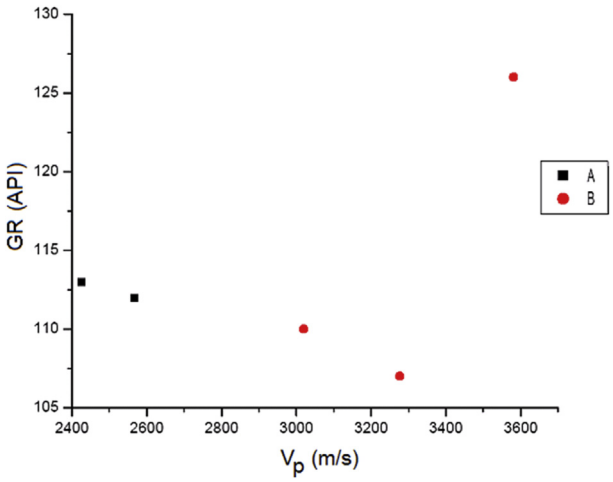

Fig. 9. The plot of GR versus P-wave velocity in comparing shales of reservoirs A and B in OBD-1 well [derived from Origin 7.0].

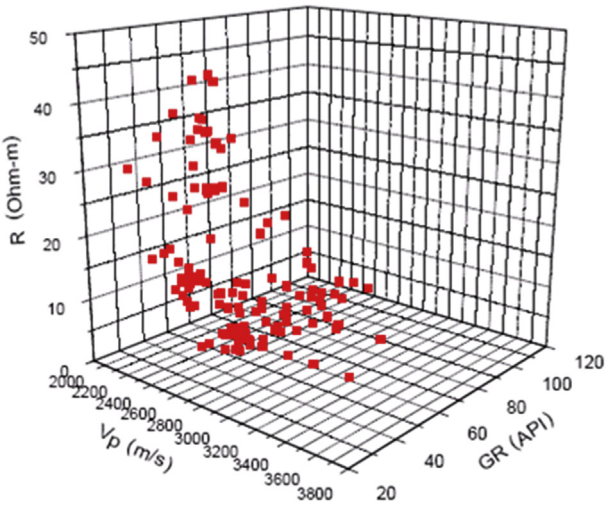

Fig. 10. The tri-variate (GR-V_p-R_{ild}) crossplot of reservoir A in OBD-1 well [derived from Origin 7.0].

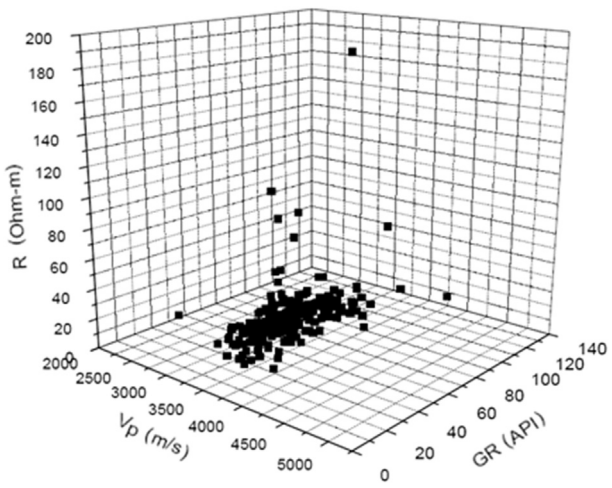

Fig. 11. The tri-variate (GR-V_p-R_{ild}) crossplot of reservoir B in OBD-1 well [derived from Origin 7.0].

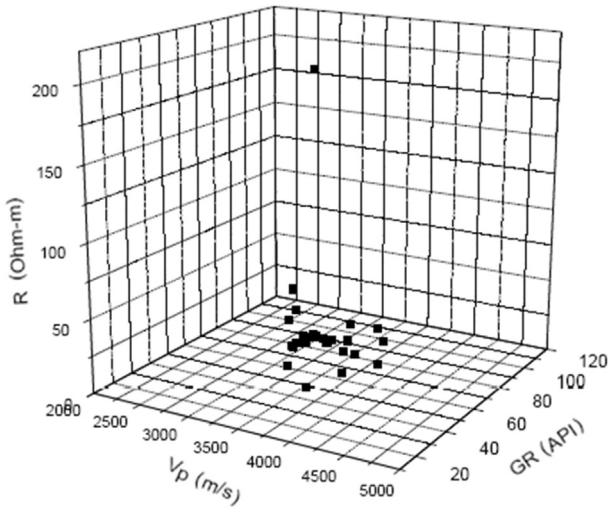

Fig. 12. The tri-variate (GR-V_p-R_{ild}) crossplot of reservoir C in OBD-1 well [derived from Origin 7.0].

To discriminate the reservoirs fully, seismic domains were introduced and crossplotted. Table 1 shows the results of mean values of rock physics parameters of reservoirs A, B, and C obtained from modeling based on the work of Olorunniwo et al. (2016).

In reservoir A, for sand, P-wave velocity ranges from 2,634 m/s to 2,860 m/s, S-wave velocity ranges from 1,570 m/s to 1,732 m/s and density ranges from 2.22 g/cc to 2.26 g/cc; for shale, P-wave velocity ranges from 2,392 m/s to 2,453 m/s, S-wave velocity ranges from 1,346 m/s to 1,383 m/s and density ranges from 2.16 g/cc to 2.18 g/cc; for brine sand, P-wave velocity is 2,798 m/s, S-wave velocity is 1,674 m/s and density is 2.25g/cc; and for hydrocarbon, P-wave velocity ranges from 2,458 m/s to 2,655 m/s, S-wave velocity ranges from 1,406 m/s to 1,579 m/s and density ranges from 1.68 g/cc to 1.74 g/cc.

Also, in reservoir B, for sand, P-wave velocity ranges from 3,509 m/s to 3,565 m/s, S-wave velocity ranges from 1,995 m/s to 2,030 m/s and density ranges from 2.38g/cc to 2.39g/cc; for shale, P-wave velocity ranges from 2,112 m/s to 2,456 m/s, S-wave velocity ranges from 786 m/s to 1,115 m/s and density ranges from 2.10g/cc to 2.18g/cc; for brine sand, P-wave velocity ranges from 3,685 m/s to 3,690 m/s, S-wave velocity ranges from 2,111 m/s to 2,124 m/s and density ranges from 2.41 g/cc to 2.42 g/cc; and for hydrocarbon, P-wave velocity ranges from 3,435 m/s to 3,501 m/s, S-wave velocity ranges from 1,932 m/s to 1,982

Table 1
Rock physics modeling of the reservoir elements.

Well Location	V_p mean	V_s mean	ρ mean	$\frac{V_p \text{ mean}}{V_s \text{ mean}}$	Lithology/Fluid Content
Reservoir A					
OBD-1	2634	1570	2.22	1.67	Sand
	2392	1346	2.16	1.77	Shale
	2614	1546	2.21	1.69	HC
	2506	1442	2.19	1.73	HC
OBD-3	2808	1596	2.25	1.75	Sand
	2655	1579	2.22	1.68	HC
OBD-14	2667	1591	2.22	1.67	Sand
	2401	1360	2.17	1.76	Shale
	2590	1530	2.20	1.69	HC
	2458	1406	2.18	1.74	HC
OBD-20	2860	1732	2.26	1.65	Sand
	2453	1383	2.18	1.77	Shale
	2798	1674	2.25	1.67	Brine
	2539	1460	2.19	1.74	HC
Reservoir B					
OBD-1	3565	2030	2.39	1.75	Sand
	2456	1115	2.18	2.21	Shale
	3501	1982	2.38	1.76	HC
	3690	2124	2.42	1.73	Brine
OBD-3	3509	1995	2.38	1.75	Sand
	2112	786	2.10	2.69	Shale
	3435	1932	2.37	1.78	HC
	3685	2111	2.41	1.74	Brine
Reservoir C					
OBD-1	4059	2384	2.47	1.7	Sand
	4006	2341	2.46	1.71	Brine
OBD-3	3620	2076	2.40	1.75	Sand

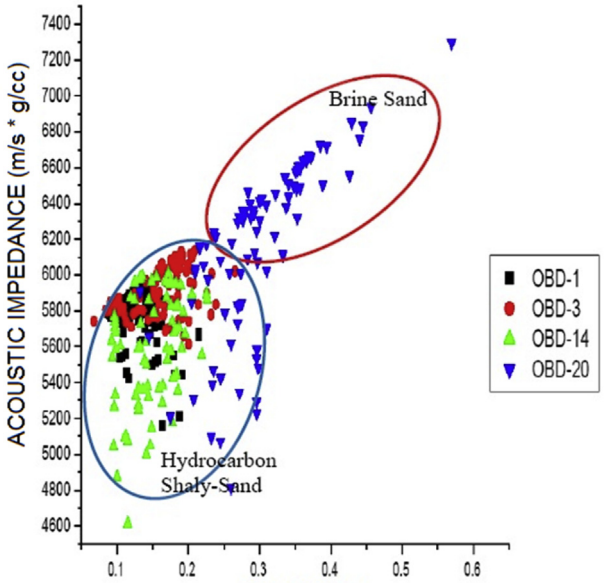

Fig. 13. Plot of Acoustic Impedance against Porosity of reservoir A [derived from Origin 7.0].

m/s and density ranges from 2.37 g/cc to 2.38 g/cc.

Lastly, in reservoir C, for sand, P-wave velocity ranges from 3,620 m/s to 4,059 m/s, S-wave velocity ranges from 2,076 m/s to 2,384 m/s and density ranges from 2.40 g/cc to 2.47 g/cc and for brine sand, P-wave velocity is 4,006 m/s, S-wave velocity is 2,341 m/s and density is 2.46 g/cc.

The plots of acoustic impedance against porosity and elastic impedance against porosity of reservoir A are displayed in Figs. 13 and 14 respectively. These crossplots discriminated brine sand from

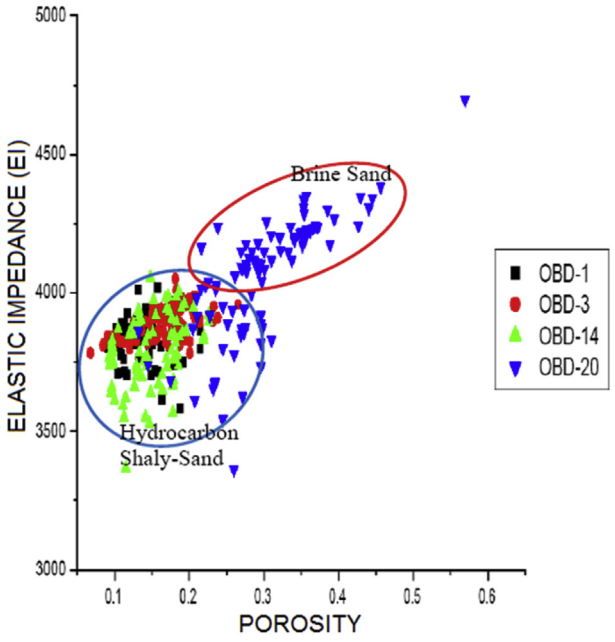

Fig. 14. Plot of Elastic Impedance against Porosity of reservoir A [derived from Origin 7.0].

hydrocarbon shaly-sand in the reservoir. Hence, this research has been able to discriminate the three existing reservoirs into four different lithofacies as well as the pore fluid contents.

5. Conclusions

Reservoir quality parameters obtained from a suite of geophysical logs were reconstructed and studied for subsurface geological features, hydrocarbon reservoir delineation and discrimination. The logs were crossplotted as bi-variate and tri-variate and studied as discriminant tools of the reservoirs in terms of lithofacies (sand, shaly-sand, sandy-shale, and shale). The comparison of bi-variate plots better displays and characterizes the texture and quality of the same lithofacies found within the three different reservoirs. The comparison of tri-variate crossplots characterizes both the lithofacies and the saturating fluid (water or oil) in the different reservoirs. The plots of acoustic impedance versus porosity and elastic impedance versus porosity confirmed the pore fluids as either brine or hydrocarbon. Therefore, seismic domains and petrophysical parameters of the three reservoirs (A, B, and C) have successfully yielded good result in discriminating these reservoirs into different lithologic units and pore fluids (brine or hydrocarbon).

Declarations

Author contribution statement

Ibukun Olorunniwo: Conceived and designed the experiments; Performed the experiments; Analyzed and interpreted the data; Contributed reagents, materials, analysis tools or data; Wrote the paper.

Sunday J. Olotu: Analyzed and interpreted the data; Contributed reagents, materials, analysis tools or data; Wrote the paper.

Olatunbosun A. Alao, Adekunle A. Adepelumi: Analyzed and interpreted the data; Wrote the paper.

Funding statement

This research did not receive any specific grant from funding agencies in the public, commercial, or not-for-profit sectors.

Competing interest statement

The authors declare no conflict of interest.

Additional information

No additional information is available for this paper.

Acknowledgements

The authors would like to thank the Department of Petroleum Resources (DPR) and the Department of Geology, Obafemi Awolowo University, Ile-Ife, Nigeria for making available for use, the data set and software respectively. The authors wish to acknowledge the valuable contributions of Professors B. D. Ako and S. B. Ojo and Associate Professor M. A. Olorunniwo (late) for conceptualizing this study.

References

Azevedo, L., Nunes, R., Correia, P., Soares, A., Guerreiro, L., Neto, G., 2014. Multidimensional scaling for the evaluation of a geostatistical seismic elastic inversion methodology. Geophysics 79 (1), M1–M10.

Azevedo, L., Nunes, R., Correia, P., Soares, A., Guerreiro, L., Neto, G., 2015. Integration of well data into geostatistical seismic amplitude variation with angle inversion for facies estimation. Geophysics 80 (6), M113–M128.

Blouin, M., Ravalec, M.L., Gloaguen, E., Adelinet, M., 2017. Porosity estimation in the Fort Worth Basin constrained by 3D seismic attributes integrated in a sequential Bayesian simulation framework. Geophysics 82 (4), M67–M80.

Castagna, J.P., Swan, H.W., Foster, D.J., 1998. Framework for AVO gradient and intercept interpretation. Geophysics 63, 948–956.

Conolly, P., 2007. Reflections on Elastic Impedance, vol. 26. The Leading Edge, p. 1360.

Evamy, B.D., Haremboure, J., Kamerling, P., Knaap, W.A., Molloy, F.A., Rowlands, P.H., 1978. Hydrocarbon habitat of tertiary Niger delta. AAPG Bull. 62, 1–59.

Frankl, E.J., Cordry, E.A., 1967. The Niger Delta oil province-recent development offshore and Onshore. In: 7th World Petroleum Congress, Mexico City, Proceedings 1B, pp. 195–209.

Hilterman, F., John, W.C., Schellhorn, R., Bankhead, B., Devault, B., 1998. Identification of Lithology in the Gulf of Mexico, vol. 17. The Leading Edge, pp. 215–217.

Lai, J., Wang, G., Chai, Y., Ran, Y., 2016. Prediction of diagenetic facies using well logs: evidences from upper triassic yanchang formation chang 8 sandstones in jiyuan region, ordos basin, China. Oil Gas Sci. Technol. 71, 34.

Maryam, H., 2017. Multivariate Stochastic Seismic Inversion with Adaptive Sampling. Doctor of Philosophy Thesis of the Department of Civil and Environmental Engineering. University of Alberta.

Mazumdar, P., 2007. Poisson dampening factor. Lead. Edge 26, 850–851.

Murat, R.C., 1972. Stratigraphy and paleogeography of the cretaceous and lower tertiary in southern Nigeria. In: African Geology: Cretaceous Rocks of Nigeria and Adjacent Areas. Ibadan University, Dept. Geology, Ibadan, Nigeria, pp. 251–265.

Olorunniwo, I., Olotu, S.J., Adepelumi, A.A., Olorunniwo, M.A., 2016. Rock Physics and AVO Mapping of Lithofacies and Pore Fluid Probabilities: Niger Delta. Society of Exploration Geophysicists (SEG) Technical Program Expanded Abstracts 2016, pp. 3112–3116.

Reijers, T.J.A., 1976. Selected Chapters on Geology. A Case Study of the Niger Delta. Published by Shell Petroleum Development Corporation, pp. 113–114.

Rotimi, O.J., Ako, B.D., Wang, Z., 2014. Reservoir characterization and modeling of lateral heterogeneity using multivariate analysis. Energy Explor. Exploit. 32 (3), 527–552.

Short, K.C., Stauble, A.J., 1967. Outline of Geology of Niger delta. AAPG (Am. Assoc. Pet. Geol.) Bull. 51, 761–779.

Teh, W.J., 2012. Improved Reservoir Characterization and Simulation of a Mature Field Using an Integrated Approach. Master of Science Thesis submitted to University of Kansas in partial fulfillment of the requirements for the degree of Master of Science.

Weber, K.J., Daukoru, E.M., 1975. Petroleum Geology of the Niger delta. Proceedings of the Ninth World Petroleum Congress. In: Geology, vol. 2. Applied Science Publishers, Ltd., London, pp. 210–221.